Rare Metal Materials and Engineering
Volume 53, Issue 7, July 2024
Available online at www.rmme.ac.cn

Science Press

Cite this article as: Li Leyu, Tian Fuzheng, Li Zhen, et al. Effect of Test Temperature on Crack Propagation Behavior of Nickel-Based Single-Crystal Superalloy[J]. Rare Metal Materials and Engineering, 2024, 53(07): 1874-1881. DOI: 10.12442/j.issn.1002-185X.20230618.

ARTICLE

Effect of Test Temperature on Crack Propagation Behavior of Nickel-Based Single-Crystal Superalloy

Li Leyu, Tian Fuzheng, Li Zhen, Zhang Jingang, Deng Zhiwei, Chen Xing, Liu Xinling

AECC Beijing Institute of Aeronautical Materials, Beijing 100095, China

Abstract: The fatigue crack propagation behavior of DD6 nickel-based single-crystal superalloy was investigated at temperatures ranging from 530 °C to 850 °C. The fatigue properties were assessed along the [001] direction, parallel to the loading axis in tension. After the fatigue crack propagation test, the fracture morphology was examined by scanning electron microscope and classified into four zones, including source zone, prefabricated crack zone, stable extension zone, and rapid extension zone. Electron backscatter diffraction was utilized to observe the profiles of plastic deformation perpendicular to the fracture. Additionally, the dislocation motion mechanism near the fracture was studied by transmission electron microscope. Results show that oxidation occurs at 650 °C under combined influences of the temperature field, stress field, and exposure time. Furthermore, due to weakened γ' phase, a significant number of consecutive dislocations form in the γ and γ' phases between 650 and 760 °C, resulting in increased oxidation of alloy. Besides, a notable decrease in fatigue propagation life can be observed at 760 °C.

Key words: nickel-based single-crystal superalloy; fatigue properties; crack propagation; dislocation motion mechanism

It has been demonstrated that aero-engine turbine blade failure primarily results from fatigue[1]. Nickel-based single-crystal superalloy is usually used as the core materials for manufacturing advanced aero-engines due to its excellent fatigue properties[2–7]. However, with the advancement of large thrust-to-weight ratio of aero-engines, the requirements for the high peripheral fatigue performance of turbine blades become increasingly stringent, such as the need for nickel-based single-crystal alloys that exhibit exceptional fatigue properties. During the development process, the anisotropy of single-crystal materials leads to significant variations in fatigue performance and fracture processes along different crystallographic directions. Current research[8–12] has shown that the [001] orientation of nickel-based single-crystal superalloy displays fatigue performance superior to [011] and [111] orientations. Ren et al[13] investigated the relationship between fatigue behavior and the microstructural evolution in [001] orientation of second-generation nickel-based single-crystal superalloy at room temperature, and found that the fatigue life of this superalloy is highly orientation-dependent and related to the modulus of elasticity and crack propagation paths. Moreover, their results show that the cyclic softening occurring in fatigue is caused by dislocation motion.

In recent years, extensive research has been conducted on fatigue crack propagation of nickel-based single-crystal superalloy through high-precision equipment[14–15]. These studies have categorized the plastic deformation modes in these alloys into planar slip and wave slip. Planar slip tends to be the dominant mode when the crack is in the first stage of fatigue, and it is characterized by a slip surface oriented at a certain angle to the load direction[16]. As fatigue progresses to the second stage, wave slip becomes dominant, in which the crack extends inward, with an extension direction gradually rotated to a plane perpendicular to the load direction. This rotation occurs as a result of the rise in the positive stress component in the direction of the applied load and a decrease in the tangential stress component, signifying the onset of the second stage of fatigue extension[17]. In addition, the fatigue performance of nickel-based single-crystal alloys is affected by temperature, this effect becomes evident in the medium temperature range, so fatigue performance increases as the temperature rises. Under high circumferential fatigue loading

Received date: October 16, 2023
Foundation item: China's National Science and Technology Major Program (J2019-VI-0022-0138)
Corresponding author: Liu Xinling, Ph. D., Researcher, AECC Beijing Institute of Aeronautical Materials, Beijing 100095, P. R. China, E-mail: liuxinling119@163.com

scenarios, 70%–80% failures occur during the fatigue crack initiation and stable expansion stages[18], and an increase in temperature further accelerates both the crack initiation and extension processes. Ma[19] conducted the behavior of small fatigue cracks in the nickel-based single-crystal superalloy DZ4 at 25, 300, and 700 °C. It was found that at 700 °C, the crack propagation behavior of this type of alloy is no longer dependent on the microstructure. Zhang et al[17] analyzed the fatigue crack propagation behavior of nickel-based single-crystal superalloy at room temperature, 300, and 600 °C. They observed that at 600 °C, planar slip becomes the dominant mode of crack propagation. Additionally, Zhou et al[20] explored the initiation and extension processes of fatigue microcrack in nickel-based single-crystal superalloy at 950 and 1050 °C. Their analyses show that at 950 °C, the alloy deformation is controlled by slip and crack-shear γ/γ'-phase cracks, whereas at 1050 °C, the alloy exhibits crack tearing in the γ-phase parallel to the loading direction and in the γ/γ' interface perpendicular to the loading direction.

However, there are few studies on the crack propagation life of DD6 nickel-based single-crystal superalloy, necessitating an investigation on the extension life in relation to temperature. This study focused on the effects of temperature on the stable extension behavior of nickel-based single-crystal superalloy and examined the relationship among temperature, product lifespan, and fracture morphology.

1 Experiment

In this study, DD6 nickel-based single-crystal superalloy was prepared in a super directional solidification furnace through the helical crystal selection method with various composition (as shown in Table 1), and crystallographic orientation was set as [001]. The as-cast single-crystal alloys were treated with a solution at 1300 °C for 6 h and underwent two-stage aging treatment at 1120 °C for 4 h and 870 °C for 32 h for eliminating eutectic phase and reducing segregation and precipitation in the γ'-strengthened phases.

The crack propagation samples were fabricated from blanks by wire EDM and automated lathes. The samples were machined along the [001] crystallographic orientation parallel to the test loading. Their shapes and dimensions are shown in Fig. 1[21]. All rough areas were checked by X-ray Lowe's back diffraction in [001] crystallographic orientation and deflection angles were ensured within 10°.

Fatigue crack propagation tests were conducted along the [001] crystallographic orientation on an MTS 370 microcomputer-controlled electronic fatigue tester at test temperatures of 530, 650, 760, and 850 °C. The tests were carried out with a stress ratio of 0.6 and a test frequency of 10 Hz in sinusoidal waveforms, and the data were recorded every 0.25 mm. Prior to testing, the samples were preheated to the designated test temperature and held for 30 min. Temperature fluctuations were controlled within ±3 °C using a temperature controller. The data recorded from the microcomputer were processed by Origin software.

The fracture occurs following fatigue loading, and the fracture morphology of the specimens was observed at different temperatures by GeminiSEM300 scanning electron microscope (SEM). A field emission SEM with Aztec data collection software was employed for electron backscatter diffraction (EBSD) characterization for the profiles perpendicular to the fracture. The EBSD samples were mechanically polished and subjected to vibration polishing with silica suspension for 6 h. Microstructural observations perpendicular to the fracture profile were performed by Talos F200X transmission electron microscope (TEM). The TEM samples were then used to prepare 5 μm×5 μm foil samples by Thermo Scientific Scios2 focused ion beam (FIB) system.

Table 1 Chemical composition of DD6 nickel-based single-crystal superalloy (wt%)

Cr	Co	W	Ta	Re	Mo	Ru	Nb	Al	Hf	C	Ni
3.0	8.5	7.0	8.0	4.0	1.2	3.0	0.6	5.5	0.2	0.008	Bal.

2 Results and Discussion

2.1 Fatigue crack propagation test

According to the Paris formula:

$$da/dN=C\Delta K^n \quad (1)$$

where a refers to crack length; N refers to cycle; K is stress-intensity factor range; C and n are crack propagation coefficients.

The fatigue crack extension rate (da/dN) curves of the nickel-based single-crystal superalloy at different test temperatures are shown in Fig. 2a, where it can be seen that they follow a linear distribution. Notably, the crack length during the stable extension stage decreases as test temperatures rise. Meanwhile, the crack propagation rate increases as test temperatures rise under the same stress

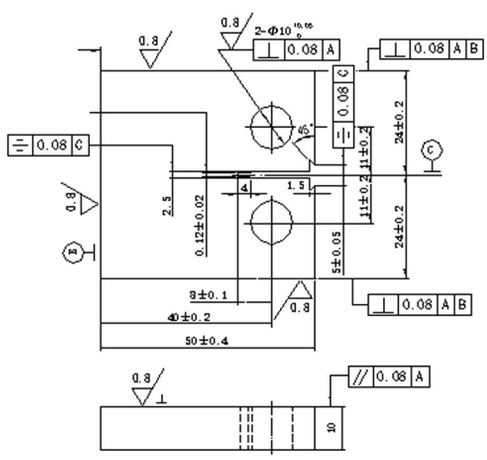

Fig.1 Shape and dimensions of fatigue crack propagation samples[21]

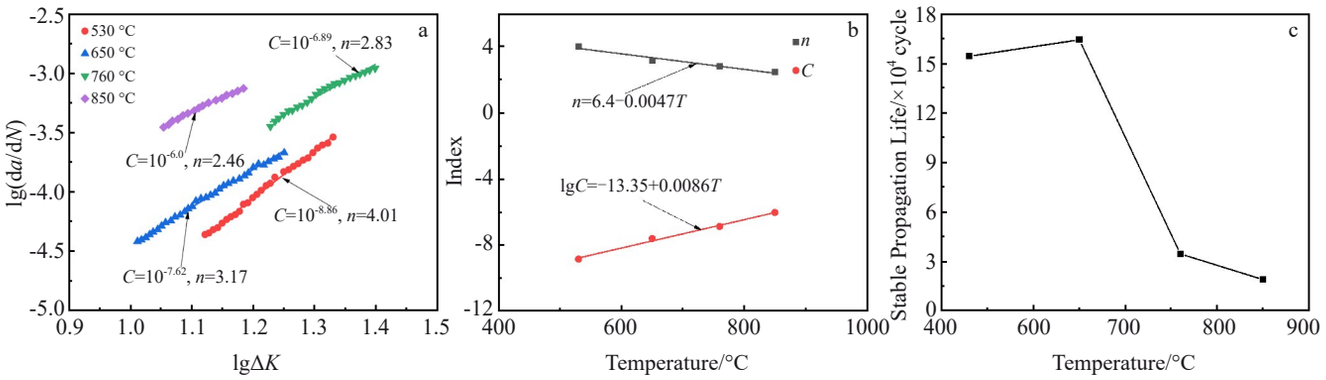

Fig.2 Fatigue-stabilized crack propagation curves of nickel-based single-crystal superalloy at different temperatures: (a) lg(da/dN) vs lgΔK, (b) change of crack propagation coefficients with temperature, and (c) fatigue crack propagation life

intensity conditions, which suggests that higher temperatures reduce the force required for stable crack propagation. Moreover, the parameters C and n in the formula above have additional changes as temperatures vary. Specifically, with increasing the temperature, C increases while n decreases, indicating that both parameters are affected by test temperature. Further analysis of the values of these parameters obtained from tests at different temperatures reveals that their changes with test temperature also follow a linear trend (Fig.2b).

Fig. 2c illustrates the fatigue-stabilized crack propagation life at different test temperatures, which is similar at 530 and 650 ° C, both exceeding 150 000 cycles. However, stable propagation life decreases to approximately 30 000 cycles at 760 °C and further reduces to a mere 18 906 cycles at 850 °C. Combining these results with Fig. 2a, it becomes evident that under the same stress intensity factor conditions, higher temperatures correspond to accelerated crack propagation rates. At temperatures of 560 and 650 ° C, the initial crack propagation rates are $10^{-4.37}$ and $10^{-4.41}$ mm/cycle, respectively, while at 760 and 850 ° C, the rates increase to $10^{-3.45}$ and $10^{-3.44}$ mm/cycle, respectively. These results indicate that the crack propagation rate rises by one order of magnitude as the temperature increases from 650 °C to 760 °C, resulting in a significant decline in fatigue stability. To follow up these findings, a series of structural characterizations were carried out to analyze the reasons behind the decrease in stability after the fatigue cracks.

2.2 Fracture morphology analysis

Fracture analysis was conducted via secondary electron imaging at low and high magnifications by SEM. The fatigue crack and its expanding fracture was divided into four zones: the source zone, the prefabricated crack zone (Fig. 3), the stable expansion zone (Fig. 4), and the rapid expansion zone (Fig. 5). In Fig. 3, it can be seen that the macroscopic fracture morphology remains similar at different temperatures, without significant differences. Due to the linear shape of the source region, multi-point stress concentration occurs along this line source, which is the result of small structural differences, leading to the formation of multiple extended prisms (indicated by the red arrows in Fig. 3). Moreover, the number of extension prisms increases with the rise in

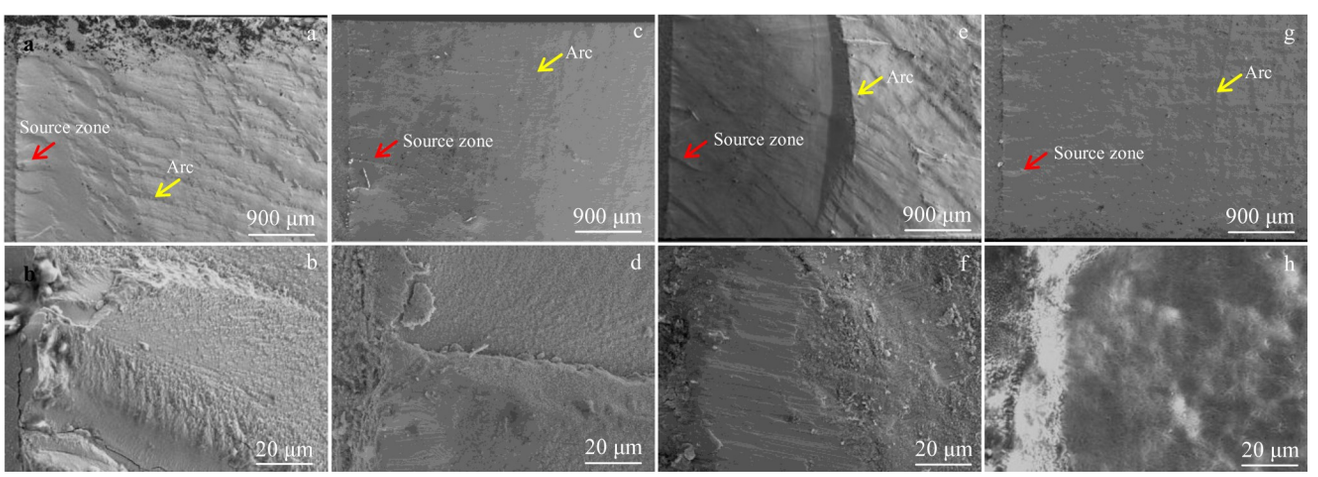

Fig.3 SEM morphologies of the source zone and prefabricated crack zone at different temperatures: (a–b) 530 °C, (c–d) 650 °C, (e–f) 760 °C, and (g–h) 860 °C

temperature, while the differences in prisms' height and width decrease. This indicates that the increase in test temperature reduces the fatigue crack propagation threshold (ΔK_{th}) and weakens the influence of the source region's shape on crack initiation. Within 2.5 mm to the source zone, a clear arc appears in the prefabricated crack zone (indicated by the yellow arrows in Fig. 3). This arc represents the morphology left by the load change during the test process when the crack propagation rate is controlled through the applied load. Furthermore, this arc marks the end of the prefabricated crack zone and signifies the beginning of the stabilized expansion zone.

In the stable expansion zone (Fig. 4), the fracture surface is flat, and at test temperatures of 650 °C or above, the fracture exhibits an X-shape deconstructive morphology (indicated in Fig. 4). Under high magnification (Fig. 4d), fine oxide particles are visible on the fracture surface at 650 °C, and as the temperature increases to 760 °C, the oxide content increases as well, resulting in the formation of a porous oxide layer (Fig. 4f). At 850 °C, the oxide layer becomes denser, large pores essentially disappear (Fig. 4h), and this phenomenon is inconsistent with existing studies on the static oxidation properties of nickel-based single-crystal superalloy. Previous study[22–23] shows that the static oxidation of nickel-based single-crystal superalloy occurs above 900 °C; however, in our fatigue crack propagation test, oxidation begins to occur at 650 °C, suggesting that the stress field plays a role in promoting oxide formation and reducing the energy required for oxide generation. Furthermore, the induced oxidation effect indicates that the significant decrease in fatigue crack stable propagation life at 760 °C instead of 650 °C is a consequence of the severe oxidation occurring at the front of the crack propagation.

Fig. 5 shows the rapid expansion zone, where solvation steps appear. At test temperatures of 560 and 650 °C, the steps are similar in size, and their overall angularity is clear. Additionally, secondary cracks can be observed between the steps, indicating that during the rapid expansion stage, the cracks undergo simultaneous cracking in multiple directions. At 760 °C, the steps become larger, and under the influence of

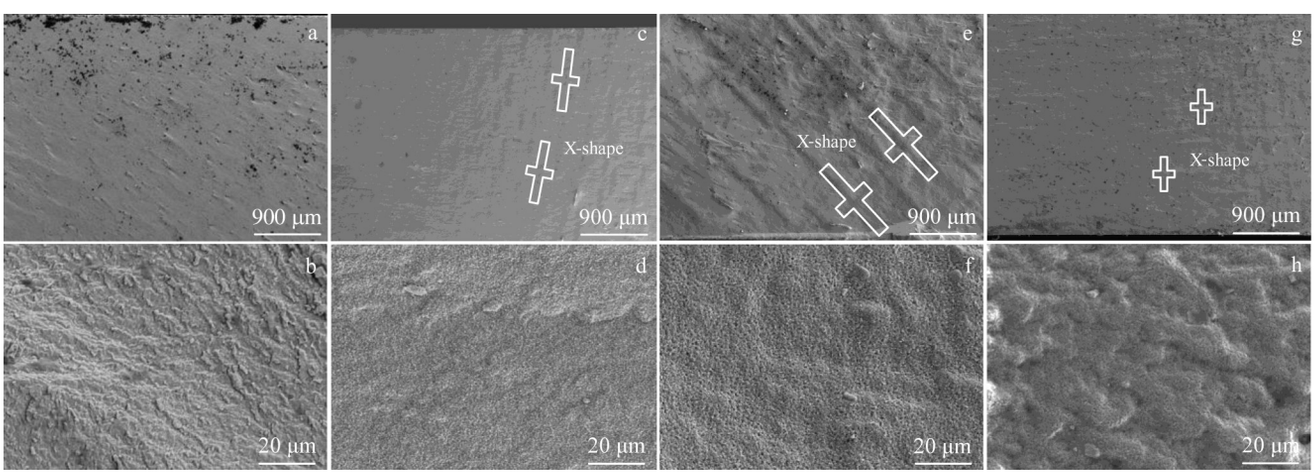

Fig.4 SEM morphologies of stable expansion zone at different temperatures: (a–b) 530 °C, (c–d) 650 °C, (e–f) 760 °C, and (g–h) 860 °C

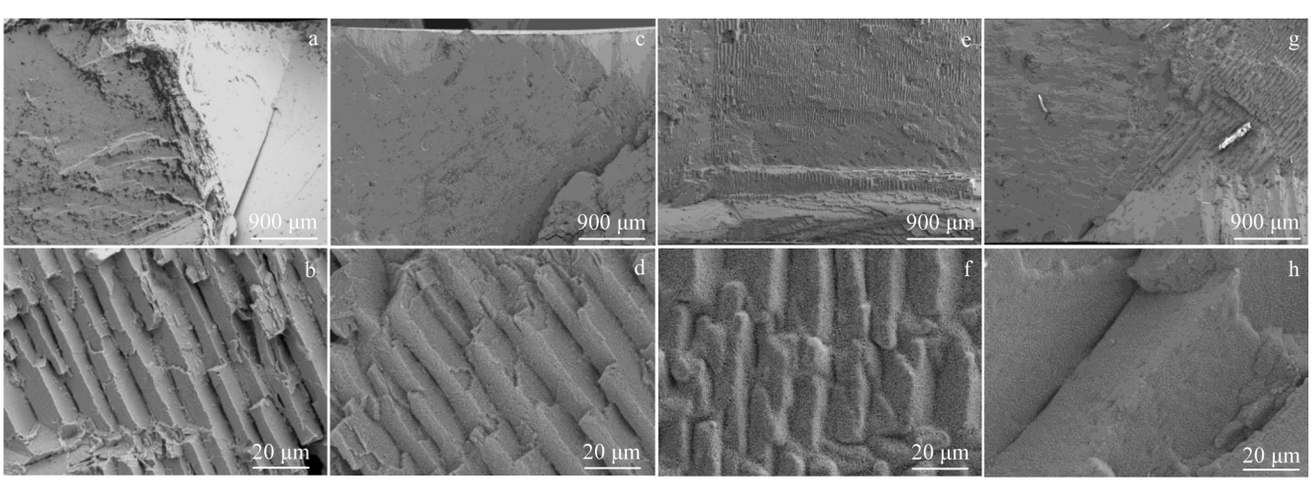

Fig.5 SEM morphologies of rapid expansion zone at different temperatures: (a–b) 530 °C, (c–d) 650 °C, (e–f) 760 °C, and (g–h) 860 °C

intensified oxidation behavior, the step surfaces become covered by porous oxidized layer. At the same time, oxidative expansion results in the disappearing of some secondary cracks, and as the temperature rises to 850 ° C, the steps become even larger. These observations suggest that at higher temperatures, cracks primarily expand in a forward direction, leading to the formation of larger step surfaces. During the rapid expansion stage from 530 °C to 850 °C, the size of these steps changes significantly and the oxide morphology gradually emerges (Fig. 5b, 5d, 5f, and 5g). These results indicate that the temperature field begins to significantly affect the crack extension at 760 °C.

2.3 Fracture mechanisms

To further explore the influence of the oxide layer and plastic deformation on stability, EBSD and TEM analyses were conducted on the fatigue crack-expanded samples at test temperatures of 650 and 760 °C. The structural changes of the fracture cross-section and dislocation motion processes were observed.

Fig. 6 shows the boundary curvature+kernel average misorientation (BC+KAM) maps obtained after characterization of the fracture cross-section via EBSD. It can be observed that an oxide layer forms on the fracture surface at both 650 and 760 °C, while an additional unidentified region becomes visible between the substrate and the oxide layer at 760 ° C, at which most of the fracture surface exhibits a polycrystalline structure due to the oxidation behavior. At the same crack length, the plastic deformation zone is significantly larger at 760 °C than that at 650 °C, and a secondary crack at approximately 45° to the fracture surface appears at 760 °C (indicated by the arrows in Fig.6b). This phenomenon is distinctly different from the condition at 650 °C, and suggests that at 760 ° C, under the influence of the ambient temperature, cracks start to expand in multiple directions. However, since the primary crack still dominates, the secondary cracks only extend a certain distance into the matrix and then terminate.

To enhance visual assessments of the oxide structure and dislocation movement processes, FIB technique was used to cut thin slices perpendicular to the fracture for TEM analysis. Fig. 7 shows the high-angle annular dark-field (HADDF) images and EDS elemental distribution of the

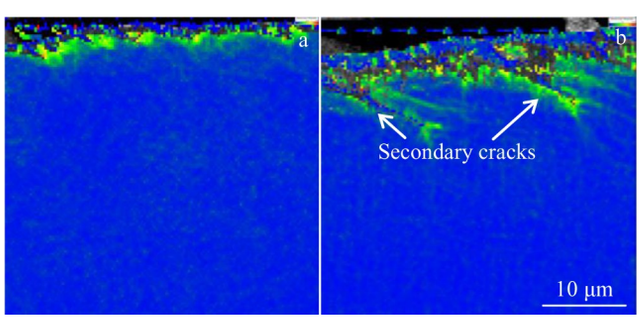

Fig.6 BC+KAM plots of nickel-based single-crystal superalloys with the same crack length at 650 °C (a) and 760 °C (b)

fracture section at different temperatures. At the test temperatures of 650 and 760 °C, the fracture cross-section can be divided into three layers: nickel oxide layer, aluminum oxide layer, and matrix layer. This is consistent with the delamination observed in Fig. 6. As the test temperature increases from 650 °C to 760 °C, the oxide layer thickness grows from about 1 μm to about 3.5 μm, following the trend observed in Fig.4.

In the middle layer (alumina layer), Ni atoms in the original square γ' phase are detached, and remaining Al and O elements form long strips of alumina. At the same time, the outermost layer exhibits single nickel oxide layer, which lacks the lattice structure of the $\gamma+\gamma'$ phase of substrate. This aligns with EBSD analysis (Fig.6) and the HADDF images (Fig.7), revealing the polycrystalline structure of the outermost layer. It also indicates that the Ni atoms in the γ' phase diffuse outward, replacing atmospheric O atoms and oxidizing on the fracture surfaces.

In Fig.8a, an adjacent γ' phase can be seen, from which Ni atoms have been stripped, as well as another γ' phase that also strips Ni atoms (indicated by the red box in Fig.8a). A channel connects these two γ' phases in the middle, and in conjunction with the EDS results, it is evident that O atoms pass through this channel into the second γ' phase that strips Ni atoms. In the magnified diffusion channel (Fig.8b), it becomes apparent that the channel passes vertically through the lattice-like γ-phase (indicated by the red arrow in Fig. 8b). Meanwhile, dislocation intersecting the γ-phase diagonally (indicated by the yellow arrow in Fig.8b) does not form a diffusion channel, suggesting that dislocations entering the γ'-phase perpendicular to the γ -phase lattice are more conducive to the formation of diffusion channels, thereby lowering the diffusion energy of the oxidation reactions.

Interestingly, in the unoxidized matrix region with plastic deformation, TEM analysis reveals that at the same crack length, the number of dislocations in the γ' phase at the test temperature of 760 ° C is much higher (Fig. 8d). These dislocations are propagated vertically from the γ phase into the γ' phase (indicated by the arrows in Fig. 8d) to form several long, parallel, straight dislocations that traverse multiple γ' and γ phases. In contrast, at 650 ° C, dislocations in the unoxidized matrix region with plastic deformation are mainly concentrated in the γ lattice, where they are severely interlaced and entangled (Fig.8c). In the γ' phase, only a small number of dislocations are encroached upon, most of which cut in the γ phase. This result suggests that the γ' phase is weakened when the test temperature increases from 650 °C to 760 °C, allowing dislocations to move more easily from the lattice-like γ phase into the cubic γ' phase. Consequently, dislocation motion intensifies, leading to a faster crack propagation rate, and in turn, a significant reduction in the fatigue crack stability. Moreover, the increase in number of dislocations of the γ' phase also accelerates the transferring of Ni atoms to the fracture surface and facilitates the internal diffusion oxidation process in the mid-temperature section. This suggests that when the test temperature reaches 760 °C,

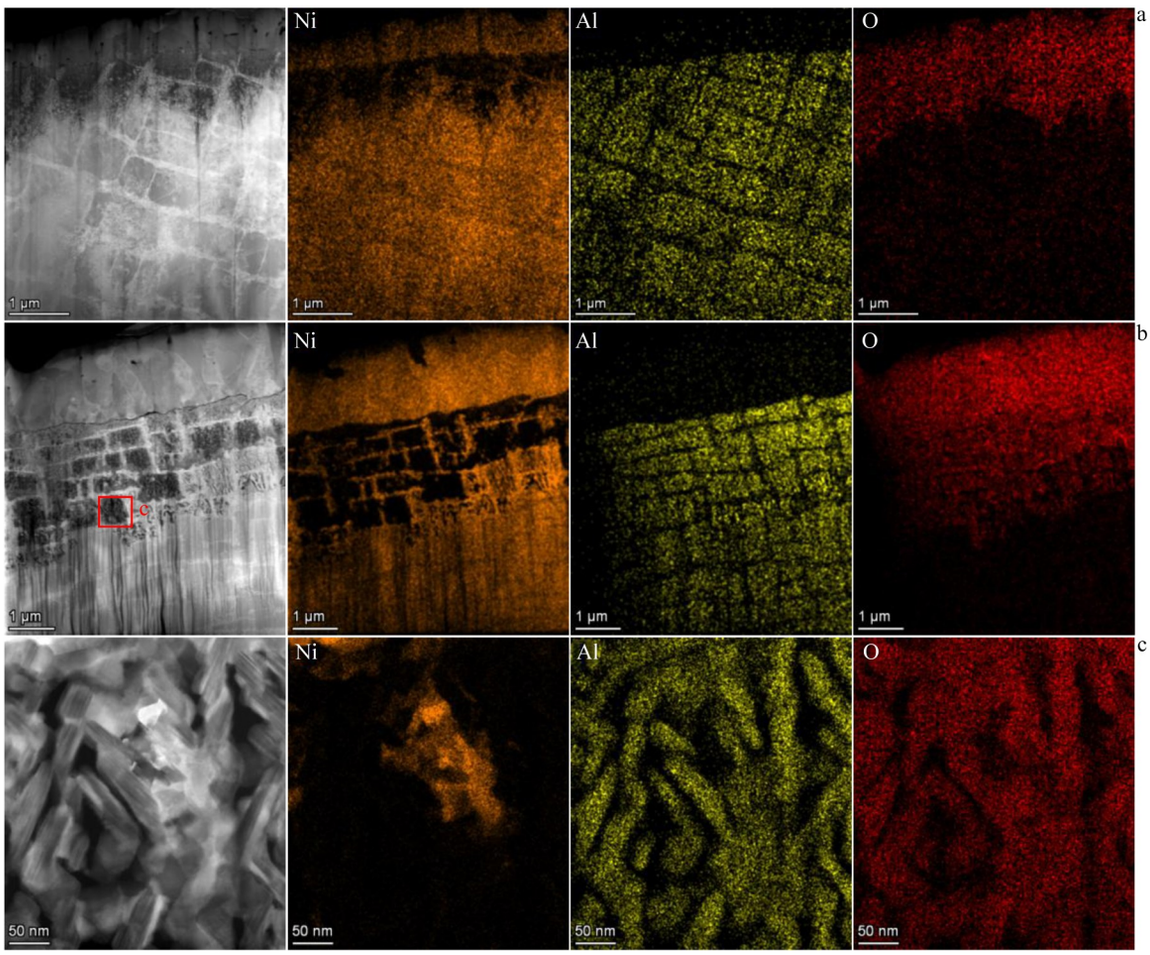

Fig.7 HADDF micrographs and EDS mappings of nickel-based single-crystal superalloy with the same crack length at 650 °C (a) and 760 °C (b-c)

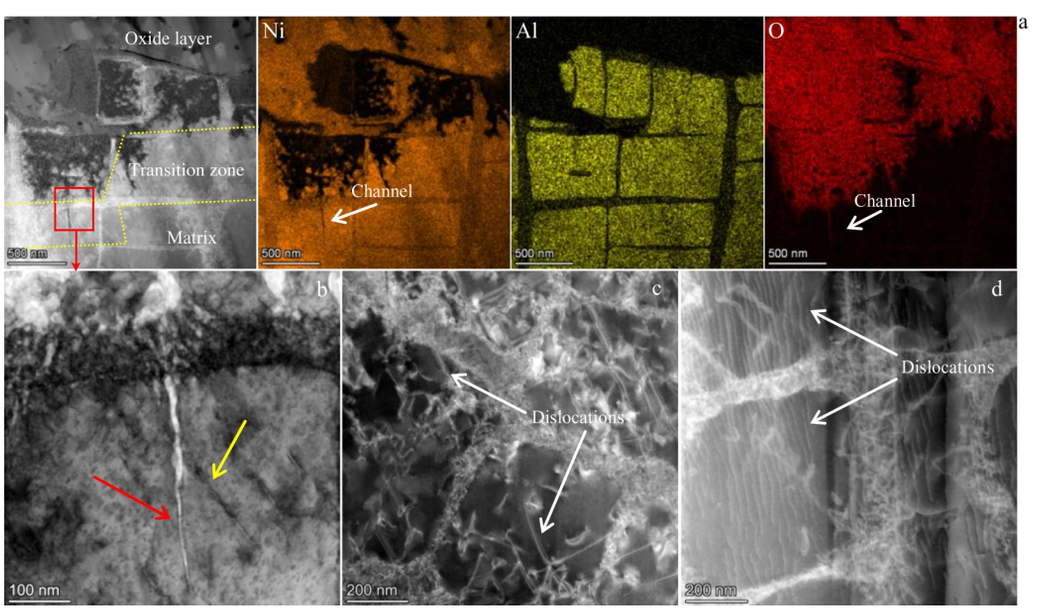

Fig.8 HADDF image and corresponding EDS mappings of oxide layer, transition zone, and matrix (a); bright field images of region in Fig.8a (b) and plastic zones at a crack length of 13.5 mm at 650 °C (c) and 760 °C (d)

oxidation occurs at the main crack front prior to crack propagation, making it difficult to achieve a stable crack propagation rate at about $10^{-4.4}$ mm/cycle. It is only when the crack propagation rate reaches about $10^{-3.4}$ mm/cycle that the

crack surface will be oxidized after crack propagation, leading to the initiation of a stable crack propagation stage that also shortens the duration of fatigue crack stability.

In summary, the fatigue crack propagation experiment conducted at different test temperatures (from 650 ° C to 760 ° C) reveals important findings about the behavior of nickel-based single-crystal superalloy. At 760 °C, the γ' phase in the alloy is weakened, resulting in dislocations entering the γ' phase more easily from the γ phase. These dislocations not only cut obliquely into the γ' phase from the γ' phase, but also significantly increase in number, entering perpendicularly to the grid-like structure of the γ' phase. This perpendicular entry by the dislocations provides diffusion channels for the exchange of element O and Ni. At 760 ° C, these diffusion channels facilitate and accelerate the oxidation reaction, leading to oxidation occurring before crack propagation, resulting in a lower crack propagation rate (about $10^{-4.4}$ mm/cycle). Consequently, it is more difficult to enter the stable extension phase, and the duration of fatigue crack stability is shortened as a result. Additionally, the increased number of dislocations entering the γ' phase results in a decrease in dislocation resistance and an acceleration of dislocation motion; that is, this accelerated motion allows the dislocations to move more easily toward the crack front, which promotes the forward motion of the crack. Consequently, the crack propagation rate is accelerated, further reducing the fatigue crack durability.

3 Conclusions

1) The fatigue crack propagation behavior of nickel-based single-crystal superalloy decreases significantly as the temperature rises. Under the same stress intensity factor, the crack propagation rate increases with increasing the temperature. When the test temperature reaches 760 ° C, the stable fatigue propagation life decreases precipitously, and at the same time, the initial crack propagation rate in the stable extension stage increases by one order of magnitude compared with that at test temperature of 650 °C.

2) The combined influence of stress field and temperature field results in the exchange of oxygen and nickel elements through diffusion channels perpendicular to the γ-phase lattice. This exchange reduces the diffusion energy of the oxidation reaction, causing oxidation to occur between 650 ° C and 760 ° C in DD6 nickel-based single-crystal superalloy. At lower crack propagation rates (about $10^{-4.4}$ mm/cycle), oxidation occurs prior to crack propagation, leading to a faster transition into the stable extension phase and a reduction in the fatigue crack durability.

3) Increasing the test temperature of nickel-based single-crystal superalloy from 650 °C to 760 °C weakens the square lattice-like γ' phase, facilitating the movement of dislocations from the γ phase into the γ' phase. As a result, dislocation motion intensifies, leading to a faster crack propagation rate and a significant reduction in fatigue crack durability.

References

1 Zhang Y, Shi H J, Gu J *et al. Theoretical and Applied Fracture Mechanics*[J], 2014, 69: 80

2 Murakumo T, Koizumi Y, Kobayashi K *et al. Superalloys*[J], 2004, 52(12): 155

3 Yue Z F, Lu Z Z, Wang X M. *Materials at High Temperatures*[J], 2002, 19(3): 147

4 Tien J K, Copley S M. *Metallurgical Transactions*[J], 1971, 2: 215

5 Mughrabi H. *International Journal of Fatigue*[J], 2013, 57: 2

6 Reed R C. *The Superalloys Fundamentals and Applications*[M]. Cambridge: Cambridge University Press, 2008

7 Pollock T M, Tin S. *Journal of Propulsion and Power*[J], 2006, 22(2): 361

8 Zhang L, Zhao L G, Roy A *et al. Materials Science and Engineering A*[J], 2019, 742: 564

9 Defresne A, Rémy L. *Materials Science and Engineering A*[J], 1990, 129(1): 45

10 Gabb T P, Welsch G, Miner R V *et al. Materials Science and Engineering A*[J], 1989, 108: 189

11 Chieragatti R, Remy L. *Materials Science and Engineering A*[J], 1991, 141(1): 1

12 Yan Wuzhu, Li Youliang, Wen Zhixun *et al*. *Rare Metal Materials and Engineering*[J], 2020, 49(6): 1854

13 Ren X, Lu J, Zhou J *et al. Materials Science and Engineering A*[J], 2022, 855: 143913

14 He Z, Zhang Y, Qiu W *et al. Materials Science and Engineering A*[J], 2016, 676: 246

15 Neu R W. *International Journal of Fatigue*[J], 2019, 123: 268

16 Lawrence F V, Jones R C. *Metal Trans*[J], 1970, 1: 367

17 Zhang Y, Shi H J, Gu J *et al. Theoretical and Applied Fracture Mechanics*[J], 2014, 69: 80

18 Miller K J. *Fatigue & Fracture of Engineering Materials & Structures*[J], 1987, 10(2): 93

19 Ma X, Shi H J. *International Journal of Fatigue*[J], 2014, 61: 255

20 Zhou J, Gao W, Yi T *et al. Materials Characterization*[J], 2023, 199: 112763

21 Tian F, Liu X. *Science of Advanced Materials*[J], 2023, 15(1): 33

22 Sato A, Chiu Y L, Reed R C. *Acta Materialia*[J], 2011, 59(1): 225

23 Hu Chunyan, Liu Xinling, Liu Changkui *et al*. *Failure Analysis and Prevention*[J], 2023, 18(1): 8 (in Chinese)

试验温度对镍基单晶高温合金裂纹扩展行为的影响

李乐宇，田福政，李　振，张金刚，邓志伟，陈　星，刘新灵
(中国航发北京航空材料研究院，北京 100095)

摘　要：研究了DD6镍基单晶高温合金从530 ℃到850 ℃的疲劳裂纹稳定扩展行为。疲劳裂纹扩展试样沿[001]方向平行于受拉的加载轴。通过扫描电子显微镜研究疲劳裂纹扩展试验后的断口形貌，并根据形貌特点分为源区、预制裂纹区、稳定扩展区以及快速扩展区。通过电子背散射衍射技术研究垂直于断口的剖面塑性变形情况。通过透射电子显微镜观察断口附近位错机制随温度的变化。结果表明，受温度场、应力场以及暴露时间的作用，在650 ℃时发生氧化，且在650 ℃至760 ℃之间，由于γ'相的弱化，在γ与γ'相中形成大量连续的位错，导致合金氧化加剧，同时760 ℃下疲劳扩展寿命显著下降。

关键词：镍基单晶高温合金；疲劳性能；裂纹扩展；位错运动机制

作者简介：李乐宇，男，2001年生，硕士生，中国航发北京航空材料研究院，北京 100095，E-mail：lileyu0110@163.com